surfaces

MDPI

Article

Electro-Oxidation of CO Saturated in 0.1 M $HClO_4$ on Basal and Stepped Pt Single-Crystal Electrodes at Room Temperature Accompanied by Surface Reconstruction

Kiyotaka Abe [1,2], Hiroyuki Uchida [1,*] and Junji Inukai [1,*]

[1] Clean Energy Research Center, University of Yamanashi, 4 Takeda, Kofu, Yamanashi 400-8510, Japan; kiyotaka.abe@jp.gs-yuasa.com

[2] Present address: GS Yuasa Corporation, 555 Sakaijuku, Kosai-shi, Shizuoka 431-0452, Japan

* Correspondence: h-uchida@yamanashi.ac.jp (H.U.); jinukai@yamanashi.ac.jp (J.I.); Tel.: +81-55-220-8185 (J.I.)

Received: 28 December 2018; Accepted: 11 April 2019; Published: 16 April 2019

Abstract: The electro-oxidation of CO on Pt surface is not only fundamentally important in electrochemistry, but also practically important in residential fuel cells for avoiding the poisoning of Pt catalysts by CO. We carried out cyclic voltammetry on Pt(111), (110), (100), (10 10 9), (10 9 8), (10 2 1), (432), and (431) single-crystal surfaces using a three compartment cell to understand the activity and durability towards the electro-oxidation of CO saturated in 0.1 M $HClO_4$. During the potential cycles between 0.07 and 0.95 V vs. the reversible hydrogen electrode, the current for the electro-oxidation of CO at potentials lower than 0.5 V disappeared, accompanied by surface reconstruction. Among the electrodes, the Pt(100) electrode showed the lowest onset potential of 0.29 V, but the activity abruptly disappeared after one potential cycle; the active sites were extremely unstable. In order to investigate the processes of the deactivation, potential-step measurements were also conducted on Pt(111) in a CO-saturated solution. Repeated cycles of the formations of Pt oxides at a high potential and Pt carbonyl species at a low potential on the surface were proposed as the deactivation process.

Keywords: CO electro-oxidation; Pt single-crystal electrodes; potential cycling; potential stepping; surface reconstruction

1. Introduction

The electrochemical oxidation (electro-oxidation) of CO, particularly on the Pt surface, is one of the most fundamental and most studied electrochemical reactions [1–3]. Many papers have been devoted to the oxidation of a pre-adsorbed monolayer of CO, often referred to as CO stripping, which usually occurs at a relatively high potential, in the 0.7 to 1.0 V range, vs. the reversible hydrogen electrode (RHE), within a narrow potential range, far from the equilibrium potential for the reaction, −0.104 V vs. RHE [4,5]. On the other hand, a current can often be observed in the lower potential region, from 0.3 to 0.5 V vs. RHE, depending both on the characteristics of the Pt surface and also to some extent on the potential at which CO was initially adsorbed. This current has been referred to as "pre-peak," "pre-wave," "pre-oxidation", or "pre-ignition" current. The origins of this current are still controversial [6–15]. With the use of an electrolyte solution saturated with CO (bulk CO), the current can flow steadily, since CO is being supplied continuously from the solution, in contrast to the case of pre-adsorbed CO, which is only a monolayer of CO adsorbed on the surface.

Strmcnik et al., using ex situ scanning tunneling microscopy (STM), presented results that have provided insight into the electro-oxidation of bulk CO in the lower potential region and found that

the presence of Pt islands and other low coordination structures on the Pt(111) surface is associated with high activity for CO oxidation at low potentials [16]. They found that, during the potential cycling process, these islands were removed. Thus, the authors proposed that the steps associated with islands, particularly at the nanometer level, are important catalytic sites, due to their low coordination number (CN). We reported the electro-oxidation of bulk CO saturated in 0.1 M $HClO_4$ on stepped Pt(111) surfaces: Pt(10 10 9) with (111) steps and Pt(20 19 19) with (100) steps (ball models in Figure 1), combined with imaging by operando STM during the electro-oxidation of bulk CO [15]. Our results, in agreement with those of Strmcnik et al. [16], suggest that the activity increases in the order: Terraces < steps < kinks < step-adatoms (single adatoms at steps), i.e., increasing activity with decreasing CN [17]. One of the most striking findings of ours was that potential cycling in the presence of CO tends to strongly favor the transformation of steps to maximize the occurrence of (111) steps, so that, for example, initially disordered (111) steps become perfectly straight, and initially straight (100) steps become zigzagged with (111) microsteps [15]. Both steps become highly inert, again due to the superb ordering of the CO adlayer across the step. The atomic-level insight, with a direct link between surface structure and electrocatalytic activity, provided a step forward in guiding the design of new, more active catalysts and electrocatalysts for CO oxidation and CO-tolerant hydrogen oxidation.

In spite of the fundamental and practical importance of the electro-oxidation of bulk CO in electrolyte solutions in the lower potential region, the reaction on single-crystal electrodes was studied only on some Pt(111)-related surfaces [12,15–18], Pt(110) [16], and Pt(100) [16,19]. However, in order to increase the reaction rate of the bulk CO electro-oxidation in the lower potential region, the reaction on surfaces with "atomically-controlled" defects also must be elucidated. The information thus obtained could be applied to the development of catalysts for residential fuel cells by avoiding the poisoning of Pt catalysts with hydrogen-rich fuel gas (reformate) produced from hydrocarbon fuels. In this work, we carried out potential cycling in a CO-saturated $HClO_4$ solution not only on basal Pt(111), (110), and (100), but also on surfaces with atomically zigzag steps of Pt(10 10 9), (10 9 8), (10 2 1), (432), and (431). On all the surfaces, the electro-catalytic activity in the pre-peak region decreased and disappeared after the potential cycling between 0.07 and 0.95 V in CO-saturated $HClO_4$. By examining cyclic voltammograms (CVs) in N_2-saturated $HClO_4$ before and after the potential cycling in the CO-saturated solution, we propose the surface reconstruction on all the Pt electrodes. Potential-step experiments were also carried out on Pt(111) to elucidate the possible mechanism of the Pt deactivation during the potential cycles.

2. Materials and Methods

Single-crystal beads of Pt, approximately 3 mm in diameter, were made by crystallization of a molten ball formed at the ends of Pt wires in a hydrogen/oxygen flame as reported previously [15,20–22]. The reflection of a laser beam from the crystal facets were used to determine the orientation of the single-crystal bead for exposing either Pt(111) or the (100) plane (Figure S1, Supporting Information). Each plane was then mechanically polished with successively finer-grade diamond pastes down to 0.25 μm with an accuracy of <0.2°. For Pt(110), (10 10 9), (10 9 8), (10 2 1), (432), and (431) planes, single-crystal beads were installed in a 4-axis X-ray diffractometer (Rigaku, Tokyo, Japan) for determining those planes prior to the mechanical polishing [15,23]. All of the samples were treated in a hydrogen/oxygen flame for two hours to eliminate surface damage caused by the mechanical polishing. Each sample was placed in an infrared image furnace filled with hydrogen [15,22], heated up to 1450 K, and gradually cooled down to 473 K, at which the gas was exchanged to Ar. The sample was taken out and placed in ultrapure water (18.2 MΩ, Milli-Q, Merck Millipore, Massachusetts, USA). The Pt electrode covered with ultrapure water was carefully and immediately transferred into an electrochemical cell filled with a 0.1 M $HClO_4$ (ultrapure grade, Kanto Chemical, Tokyo, Japan) solution saturated either with N_2 or CO. The continuous potential cycling in a CO-saturated solution was carried out between 0.07 and 0.95 V at 50 mV s^{-1} (35.2 s for each cycle), whereas the CVs in a N_2-saturated solution were recorded between 0.05 and 0.95 V at 50 mV s^{-1} before and after the 30 potential cycles in a CO-saturated solution. On Pt(111), the potential-step measurements

were carried out. The sample was first exposed to a CO-saturated solution at 0.05 V for 2 min. Then, the potential was stepped and kept at 0.60 V for 6 min, then at 0.95 V for 2 min, and back at 0.60 V for 6 min. This 16-min procedure was repeated 26 times, and the current density was simultaneously measured. All electrochemical measurements were carried out at 293 K using a potentiostat (PGSTAT128N with an analog scan module, Metrohm Autolab, Herisau, Switzerland) with the hanging meniscus method in a three-compartment electrochemical cell (Figure S2, Supporting Information). All electrode potentials in this work are referred to the RHE.

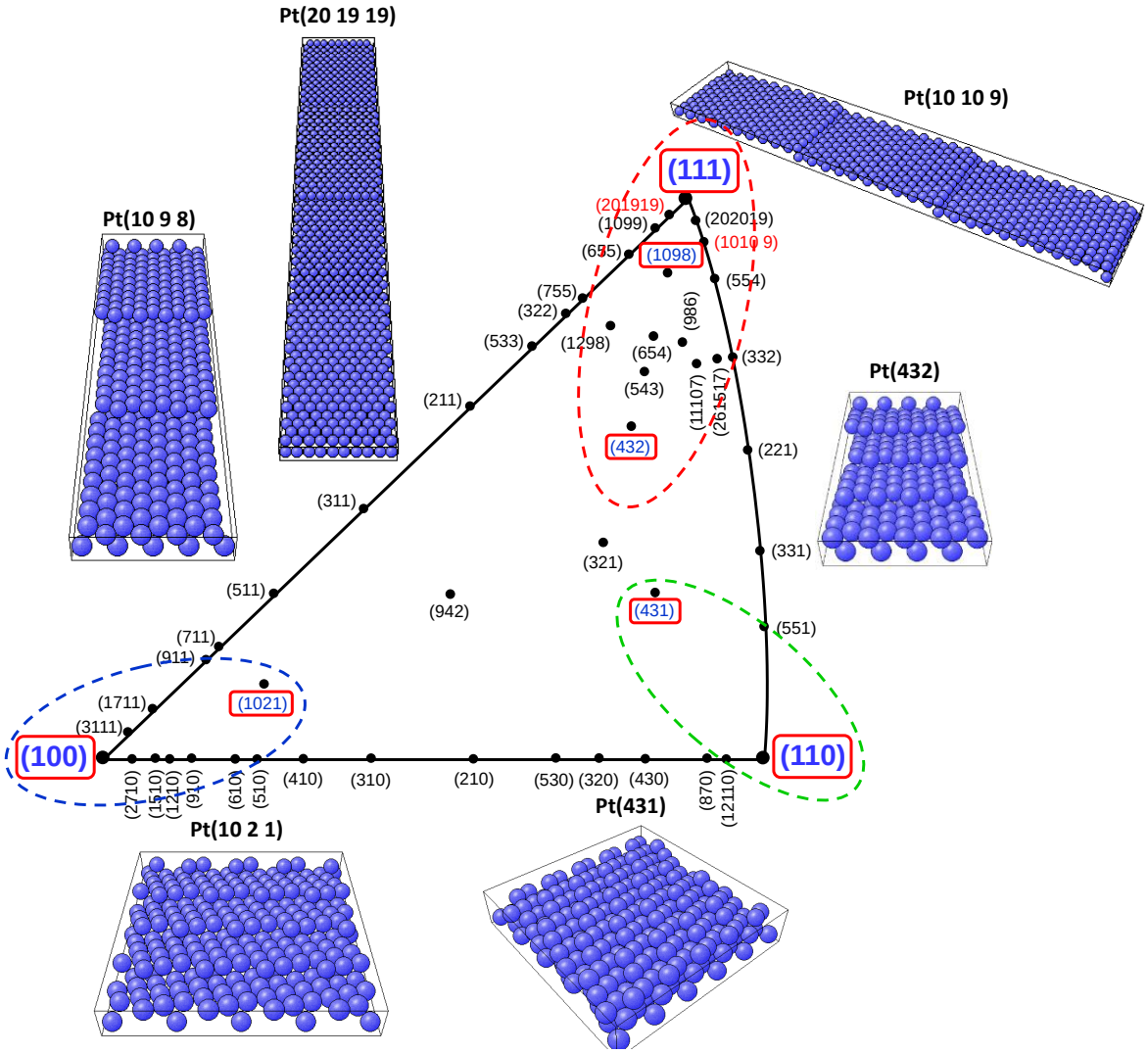

Figure 1. Unit triangle of stereographic projection, showing the location of various Pt surfaces. Ball models of (20 19 19), (10 10 9), (10 9 8), (10 2 1), (432), and (431) planes are depicted in blue.

3. Results and Discussion

3.1. CVs on Pt Single-Crystal Surfaces in CO-Saturated $HClO_4$

The continuous potential cycling was carried out on Pt samples in a 0.1 M $HClO_4$ solution saturated with CO. After 30 cycles, the steady-state CV curves showed no change on all samples. Figure 2a-1,b-1,c-1 show CVs obtained in N_2-saturated $HClO_4$ before (black line) and after (red line) the 30 potential cycles in CO-saturated $HClO_4$ on Pt(111), (10 9 8), and (432), respectively. Those three planes are related to Pt(111) (Figure 1). On the Pt(111) surface used in this study, a small amount of (111) steps existed as reported in our previous study [15]. On (10 9 8) and (432), ideally, steps are composed of alternating (111) and (100) steps with one-atomic width (Figure 1). The average step density was estimated to be 1/9 on Pt(10 9 8) and 1/4 on Pt(432). The hydrogen and hydroxide

adsorption/desorption regions are seen at potentials lower and higher than 0.5 V, respectively. A subtle growth of the spikes at around 0.8 V was seen on Pt(111), which is indicative of a small increase in the flatness of the terraces [15,23]. On (10 9 8) and (432), very small changes are observed at the peaks observed in both hydrogen and hydroxide adsorption/desorption regions. In H_2SO_4 solutions, the peaks around 0.13 and 0.28 V have been reported to be associated with (110) and (100) planes [23]. If this is also the case in $HClO_4$, both surfaces had characteristics of (110) and (100) planes, which is evident from the ball models shown in Figure 1, although detailed structural analysis should be carried out based on techniques, such as in situ STM [15]. Figure 2a-2,b-2,c-2 show CVs on Pt(111), (10 9 8), and (432), respectively, obtained in a 0.1 M $HClO_4$ solution saturated with CO. The potential was swept repetitively from 0.07 to 0.95 V with 30 cycles at a scan rate of 50 mV s^{-1}. Only the CVs for positive-going scans are shown in the figures. Figure 2a-3,b-3,c-3 are enlargements of the lower potential range in 2(a-2), 2(b-2), and 2(c-2), respectively. The current due to CO oxidation initially commenced at 0.37 V on Pt(111), at 0.43 V on (10 9 8), and at 0.42 V on (432). A broad anodic oxidation feature, often termed a "pre-peak", but referred to more properly as "low-potential CO oxidation current", at about 0.5 to 0.7 V was seen, followed by a sharp spike at around 0.8 V, known as the main peak. After 30 cycles, practically no current was seen at the lower potential region than the main peak on all surfaces. Because the CVs in the N_2-saturated $HClO_4$ solution (Figure 2a-1,b-1,c-1) were similar before and after the potential cycles, the surface structures might not be drastically changed; only atomic structures of steps might have been changed as reported on Pt(111) and stepped Pt(111) with either (111) or (100) steps [15]. In the case of (111) steps on Pt(111), the increase of the step density increase the "low-potential CO oxidation current" [15]. However, for Pt(10 9 8) and (432), the increase in the step density by a factor of 2.3 rather decreased the current (Figure 2). This could be explained by the difference in the actual configurations at the steps at Pt(10 9 8) and (432), although in the ideal models shown in Figure 1, the steps are identical on both surfaces. The ratio of the peak currents at 0.13 and 0.28 V are different on Pt(10 9 8) and (432) in an N_2-saturated solution, which also indicates that the step structures on Pt(10 9 8) and (432) are different. Interestingly, the decrease of the "low-potential CO oxidation current" was similar on Pt(111) and (10 9 8). Therefore, the step structure on Pt(10 9 8) might be similar to that on Pt(111).

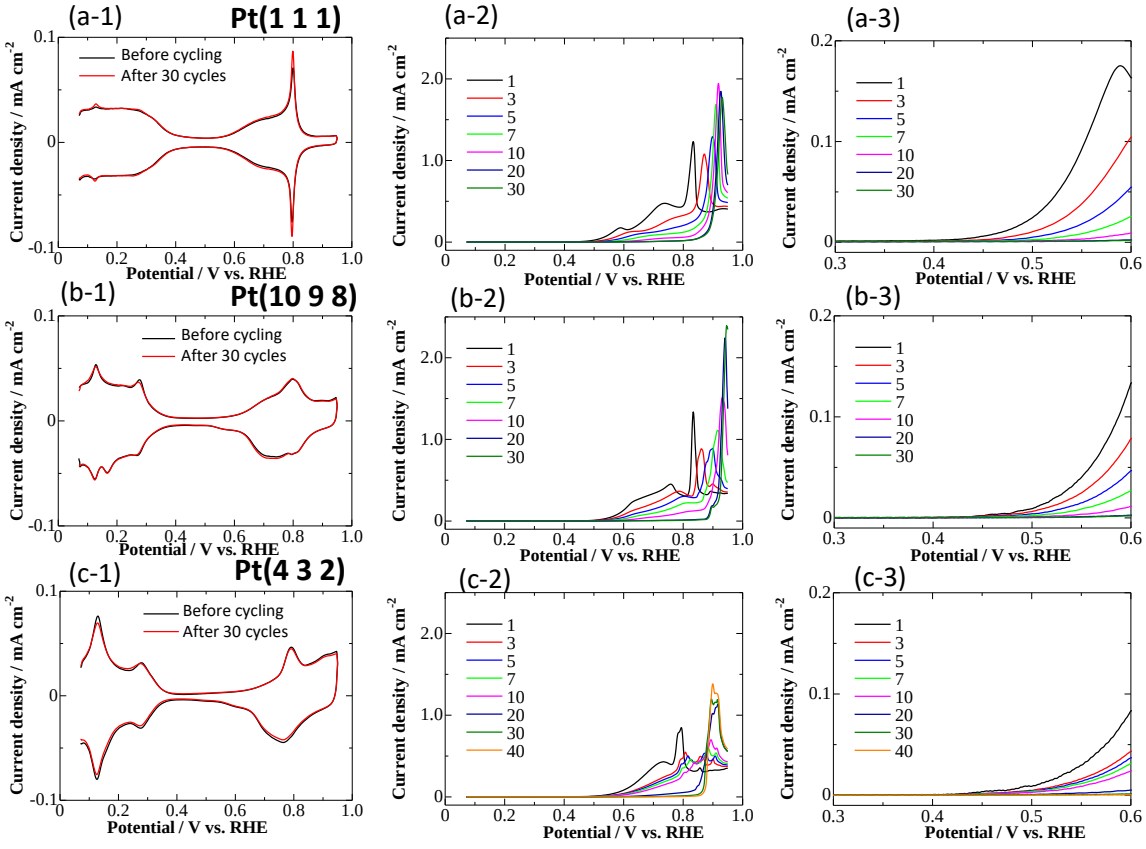

Figure 2. (**a-1**), (**b-1**), and (**c-1**) show CVs obtained in N_2-saturated $HClO_4$ before (black line) and after (red line) the 30 potential cycles in CO-saturated $HClO_4$ on Pt(111), (10 9 8), and (432), respectively. Scan rate = 50 mV s^{-1}. (**a-2**), (**b-2**), and (**c-2**) show the results of the CVs on Pt(111), (10 9 8), and (432), respectively, obtained in a 0.1 M $HClO_4$ solution saturated with CO. Scan rate = 50 mV s^{-1}. (**a-3**), (**b-3**), and (**c-3**) are enlargements of the lower potential range in (**a-2**), (**b-2**), and (**c-2**), respectively.

Figure 3 shows CVs on Pt(110) and (431). Pt(431) is oriented with (110), ideally with only a 2-atomic width of the (111) terraces (see Figure 1). On Pt(110), the CV in N_2-saturated $HClO_4$ before the potential cycles (black line in Figure 3a-1) was identical to those reported previously [24–26]. By in situ STM, the surface prepared in the same manner as in this study was reported to consist of parallel atomic rows aligned along the [110] direction, with an atomically-resolved (1 × 1) structure [22]. After the potential cycles in CO-saturated $HClO_4$, many characteristic peaks in the CV were lost (red line in Figure 3(a-1)). Therefore, the surface structure must be largely reconstructed. The lost peaks might indicate a reconstruction into "dim" surface structures with no distinct steps and terraces after the potential cycles. The CVs on Pt(431) in N_2-purged 0.1 M $HClO_4$ obtained before and after the potential cycles in a CO-saturated solution showed a large peak at 0.1 V in the hydrogen adsorption/desorption region. Little change was observed before and after the potential cycles (Figure 3b-1) in contrast to the results on Pt(110) (Figure 3a-1). This is indicative of little change in the surface structure after the potential cycles on Pt(431), because of the unique surface morphology of Pt(431); the defect sites were densely and uniformly arranged on the surface, which cause the surface energy to be rather small. Figure 3a-2,b-2 show CVs on Pt(110) and (431) obtained in a 0.1 M $HClO_4$ solution saturated with CO, respectively. Figure 3a-3,b-3 are enlargements of the lower potential ranges. On Pt(110), a small "low-potential CO oxidation current" with an onset of 0.35 V was seen to decrease as the potential was cycled. On Pt(431), the "low-potential CO oxidation current" commencing at 0.40 V during the first scan was comparable to those on Pt(111)-related surfaces (Figure 2), which abruptly decreased even at the second cycle. Because we expected a large "low-potential CO oxidation current" on this highly-defected surface, the results were surprising. In our previous paper, we concluded that bulk CO electro-oxidation at potentials lower than 0.5 V proceed at surface sites not fully covered by CO molecules [15]. If this reaction model is correct, a small amount of sites not covered by CO existed before the potential cycles on Pt(431), but the sites quickly disappeared and the surface was efficiently covered by CO during the first cycle. To conclude, bulk CO electro-oxidation at low potentials is not necessarily high at a surface with many defects; the absorption structure of CO molecules must be simultaneously taken into account, too.

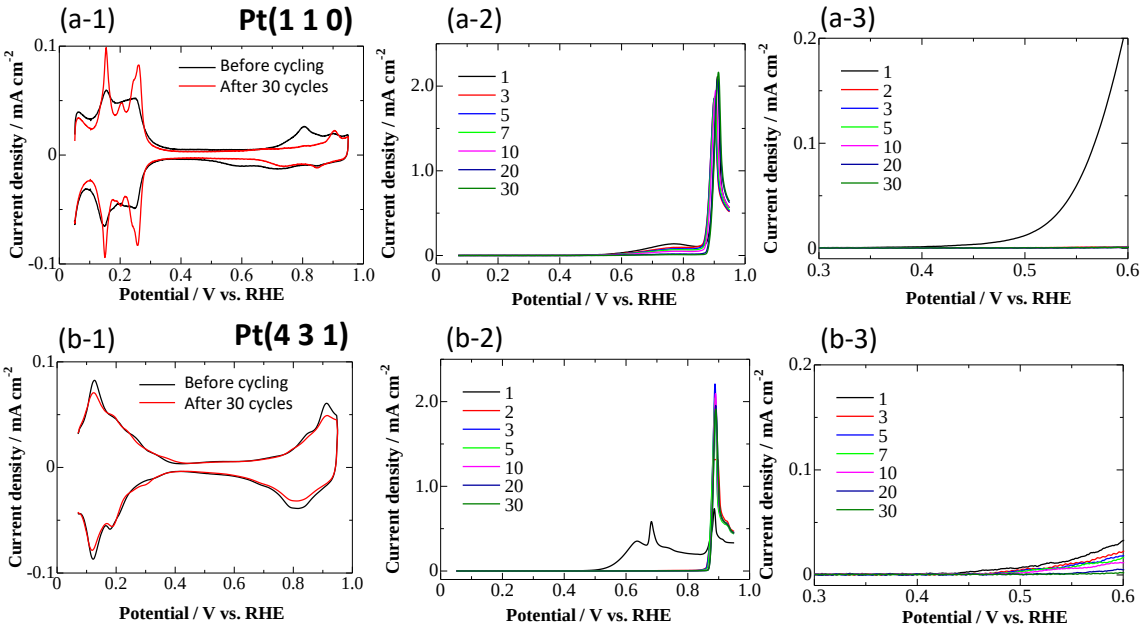

Figure 3. (**a-1**) and (**b-1**) show CVs obtained in N_2-saturated $HClO_4$ before (black line) and after (red line) the 30 potential cycles in CO-saturated $HClO_4$ on Pt(110) and (431), respectively. Scan rate = 50 mV s^{-1}. (**a-2**) and (**b-2**) show the results of the CVs on Pt(110) and (431), respectively, obtained in a 0.1 M $HClO_4$ solution saturated with CO. Scan rate = 50 mV s^{-1}. (**a-3**) and (**b-3**) are enlargements of the lower potential range in (**a-2**) and (**b-2**), respectively.

Figure 4 shows CVs on Pt(100) and (10 2 1). On (10 2 1), the steps are ideally all (111), but kinks are located on the four-fold sites of Pt(100) (CN = 6), which are unique to this surface. On Pt(100), the CV in N_2-saturated $HClO_4$ before the potential cycles (black line in Figure 3(a-1)) was identical to those reported previously [26]. In situ STM images with Pt atoms forming (100)–(1 × 1) structure were already reported on the surfaces after the similar sample preparation procedures [27,28]. On Pt(100), the electro-oxidation of bulk CO commenced at 0.29 V, the lowest potential among the surfaces investigated in this study. On Pt(10 2 1), the onset potential for CO oxidation was 0.35 V, higher by 0.06 V than on Pt(100). After the potential cycles in CO-saturated solution, the shape of the CVs changed on both surfaces [15], but not in an extinctive manner as on Pt(110). Although the onset potential was very low on Pt(100), the "low-potential CO oxidation current" became non-observable even at the second cycle. Therefore, the sites for the electro-oxidation of bulk CO were extremely active, but unstable on Pt(100). Since the onset potential of Pt(100) was lower than on Pt(10 2 1) with kinks, the active sites on Pt(100) might be those with lower CN than kinks, or isolated Pt adatoms (CN = 4) or clusters composed of a few Pt atoms (CN = 4–6) as proposed previously [15,16,27,29]. However, as already mentioned, the reaction rate of the electro-oxidation of bulk CO is not determined only by the numbers of sites with smaller CNs, but also by the structure of the CO adlayer [15,28].

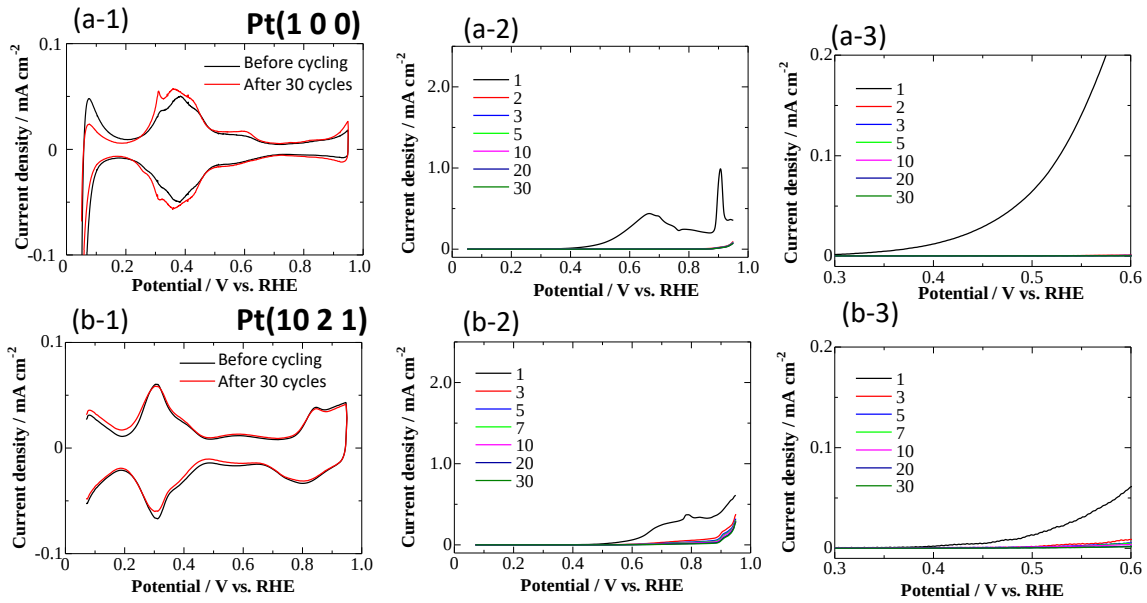

Figure 4. (**a-1**) and (**b-1**) show CVs obtained in N_2-saturated $HClO_4$ before (black line) and after (red line) the 30 potential cycles in CO-saturated $HClO_4$ on Pt(100) and (10 2 1), respectively. Scan rate = 50 mV s^{-1}. (**a-2**) and (**b-2**) show the results of the CVs on Pt(100) and (10 2 1), respectively, obtained in a 0.1 M $HClO_4$ solution saturated with CO. Scan rate = 50 mV s^{-1}. (**a-3**) and (**b-3**) are enlargements of the lower potential range in (**a-2**) and (**b-2**), respectively.

Table 1. Onset potentials for bulk CO electro-oxidation in 0.1 M $HClO_4$ saturated with CO.

	Pt(111)-oriented			**Pt(110)-oriented**		**Pt(100)-oriented**	
	Pt(111)	**Pt(10 9 8)**	**Pt(432)**	**Pt(110)**	**Pt(431)**	**Pt(100)**	**Pt(10 2 1)**
Onset potential / V vs. RHE	0.37	0.43	0.42	0.35	0.40	0.29	0.35

In Table 1, the onset potentials during the first potential scans are listed on all the Pt electrodes. It is clear that the numbers of defects shown in the ideal structures (Figure 1) are not related to the order of the onset potentials. This might be indicating that the structures of actual active sites are mostly not as those shown in Figure 1. In our previous paper, it was reported that the active sites on Pt(111) existed preferentially at steps and were very small in number [15]. Even by using single-crystal surfaces with zigzag steps in this study, the active sites for bulk CO electro-oxidation were not increased. Interestingly, the onset potentials were always lower on the basal planes rather than on stepped surfaces on Pt(111)-, Pt(110)-, and Pt(100)-oriented surfaces. This might imply that those highly-active sites were adatoms or clusters, having low CNs, on the basal planes or at steps, as discussed on Pt(100). The instability of those sites is discussed in the following section.

3.2. Potential Stepping on Pt(111) in CO-Saturated $HClO_4$

On all Pt surfaces with different types of defects, the current for the CO electro-chemical oxidation in the lower potential region disappeared after potential cycles. By ex situ [16] and operando [15] STM, it has been reported that the loss in the activity for the CO electro-oxidation was related to the transformation of Pt surface structures by a reduction of the surface defects [16]. In our previous report, the deactivation of the electrodes was connected with the formation of the single atomic Pt species [15]:

Anodic scan (up to 0.95 V):

$$Pt(OH)_2 \rightarrow PtO_2 + 2H^+ + 2e^- \quad (1)$$

$$PtO + H_2O \rightarrow PtO_2 + 2H^+ + 2e \quad (2)$$

Cathodic scan (lower than 0.80 V):

$$PtO_2 + 2H_2O + 4H^+ + 2e^- \rightarrow Pt(H_2O)_4^{2+} \quad (3)$$

$$Pt(H_2O)_4^{2+} + 4CO \rightarrow Pt(CO)_4^{2+} + 4H_2O \quad (4)$$

$$Pt(CO)_4^{2+} + 2e^- \rightarrow Pt(CO)_2 + 2CO \quad (5)$$

At 0.95 V, bulk CO electro-oxidation and the formation of Pt oxides must competitively proceed on surface, where Pt atoms with low CNs are expected to be easily oxidized. When the potential was scanned in the cathodic direction, those (single or several atomic) oxides were reduced to $Pt(CO)_4^{2+}$ or $Pt(CO)_2$ on the surface. The single atomic Pt species, either as $Pt(CO)_4^{2+}$ or $Pt(CO)_2$, would then have the opportunity to redeposit at the nearby site in an energetically favorable configuration. In the previous section, the active sites on Pt(100) were proposed as adatoms or atomically small clusters. $Pt(CO)_4^{2+}$ or $Pt(CO)_2$ could be preferentially formed from those isolated Pt adatoms with small CNs, therefore, those active sites should be very unstable as shown in Figure 4.

In addition to CV measurements (Figures 2–4), we carried out potential stepping [18,30]. The Pt(111) surface was used because the atomically-resolved structural information was obtained only on Pt(111)-related single-crystal electrodes during bulk CO electro-oxidation [15]. The sample was exposed to a CO-saturated solution at 0.05 V for 2 min, stepped to 0.60 V and left for 6 min, to 0.95 V for 2 min, then back to 0.60 V for 6 min. The current density obtained at 0.60 V was chosen as a measure for the CO electro-oxidation in the lower potential region. This 16 min procedure was cycled 26 times. The current density was simultaneously recorded. Figure 5 shows the current density during the potential-step cycles. The current density was initially 0 mA cm^{-2} at 0.05 V, then abruptly increased to 0. 17 mA cm^{-2} as the potential was stepped to 0.60 V at 2 min (black line in Figure 5). The current density slowly decreased to 0.06 mA cm^{-2} during the 6-min interval. Subsequently, the current density increased sharply to 0.5 mA cm^{-2} upon the potential step to 0.95 V at 8 min and decreased to 0.25 mA cm^{-2} at 10 min. When the potential was switched down to 0.60 V at 10 min, after a cathodic spike, the current density very slowly decreased down to 0.02 mA cm^{-2} in 6 min. Interestingly, after the sample was again kept at 0.05 V for 2 min, the current density jumped to 0.14 mA cm^{-2} accompanied by the potential step to 0.60 V, slightly lower than the first jump (0. 17 mA

cm^{-2}). The current decreased to 0.04 mA cm^{-2} at 0.60 V after 6 min (or at 8 min) in the second cycle. Indeed, the current density at 0.60 V between 2 and 8 min in the (N + 1)th (N = 1 to 25) cycle was always larger than that at 0.60 V between 10 and 16 min in the Nth cycle, showing the partial recovery of the activity in the lower potential region. Between 2 and 8 min and between 10 and 16 min at 0.6 V, the current density at the corresponding period in the (N + 1)th cycle was always smaller than that in the Nth cycle (Figure 5), showing a continuous deactivation. Between 8 and 10 min at 0.95 V, the current density was not in an order. This discrepancy at 0.95 V might be due to the diffusion of the solution not controlled in the experimental configuration shown in Figure S2. Rotation disk electrode measurements are needed for detailed analyses.

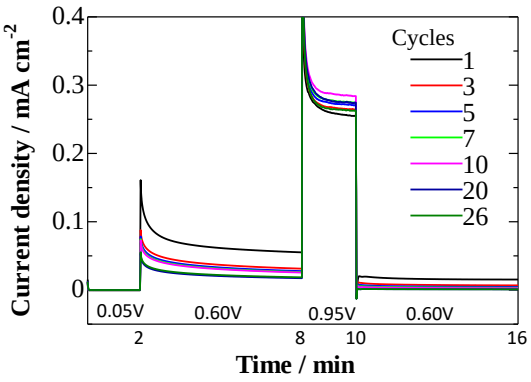

Figure 5. Current density obtained on Pt(111) during the potential steps in CO-saturated $HClO_4$.

Operando STM measurements were carried out on Pt(111) in CO-saturated $HClO_4$ at 0.05, 0.60, and 0.95 V. At 0.95 V, the atomic arrangements were not able to be obtained because of the continuous electro-oxidation of CO, although the terraces were observed to be flat. At 0.05 and 0.60 V, the (2 × 2)-3 CO structure was steadily observed as shown in Figure 6. Therefore, the CO adlayer was rigid and stable between 0.05 and 0.60 V. It is also understood that the bulk CO electro-oxidation at 0.6 V proceeded at steps. The reconstruction of steps without potential cycling either at 0.05 or 0.60 V was not observed by STM, indicating that the mobile sites were very limited in number.

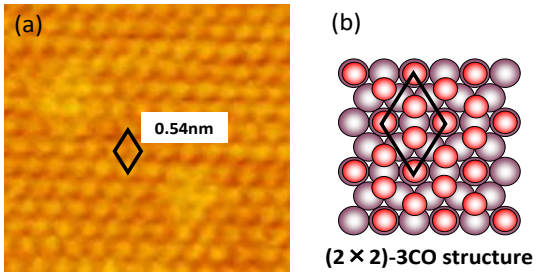

Figure 6. (**a**): Operando STM image of a CO adlayer on a Pt(111) terrace forming (2 × 2)-3CO obtained in 0.1 M $HClO_4$ saturated with CO at 0.60 V vs. RHE during the CO electro-oxidation. A unit cell is depicted as a rhombus. The length of the sides was 0.54 nm, and the angle was 120°. (**b**): Structural model of a (2 × 2)-3CO adlayer on Pt(111)–(1 × 1). The red and purple circles represent CO molecules and Pt atoms, respectively.

Based on the results obtained above, the deactivation processes during the potential steps were modeled.

1. At 0.95 V, the surface was continuously deactivated by the simultaneous formation of surface oxides (Figure 5, Equations (1) and (2)). Pt adatoms or Pt clusters with low CNs were preferentially oxidized. Those oxidized species were immobile on the surface.

2. The current density at 0.60 V, after being treated at 0.95 V, became much smaller (Figure 5) along with the formation of a stable CO adlayer on the terraces (Figure 6). $Pt(CO)_4^{2+}$ (Equation (4)) or $Pt(CO)_2$ (Equation (5)) species were also formed after the potential step by the reduction of the (single or several atomic) Pt oxides. We believe that, at least partially, $Pt(CO)_4^{2+}$ remained on the surface at 0.60 V after the potential step from 0.95 V, because Pt oxides were not completely reduced to metal Pt at 0.60 V after going through 0.95 V, as seen in the CVs obtained in pure $HClO_4$ (Figures 2–4). Because the reactivity did not change very much at 0.60 V, the surface morphology did not change either. Therefore, the planar and electronically charged $Pt(CO)_4^{2+}$ species, inactive towards the bulk CO electro-oxidation, might be immobile on the Pt surface.

3. At 0.05 V, all $Pt(CO)_4^{2+}$ species became $Pt(CO)_2$. The current density at 0.60 V after treatment at 0.05 V became larger than that after treatment at 0.95 V (Figure 5), because of the formation of $Pt(0)(CO)_2$ from $Pt(II)(CO)_4^{2+}$; metallic Pt species can be active towards bulk CO electro-oxidation. The reaction rate, on the other hand, was continuously lowered at 0.60 V. This is because of the deposition of mobile $Pt(CO)_2$ at the energetically favorable adjacent site on the surface, thus lowering its CN and eventually its reaction activity.

4. Repeating the treatments at 0.05 and 0.95 V gradually decreased the reaction rate of the bulk CO electro-oxidation in the lower potential region (Figure 5). The potential cycling between 0.07 and 0.95 V much enhanced the deactivation process on Pt electrodes (Figures 2–4) compared with the potential-step treatment (Figure 5), possibly because of the continuous morphological change during the potential cycling.

4. Conclusions

The electro-oxidation of CO was investigated on Pt single-crystal electrodes with different surface orientations in CO-saturated 0.1 M $HClO_4$. On all Pt(111)-, (110)-, and (100)-oriented surfaces, the "low-potential CO oxidation current" disappeared during the potential cycles between 0.07 and 0.95 V in a CO-saturated solution. During the potential cycles, the surface structures changed. On Pt(111)-oriented surfaces, the reconstruction proceeded only at steps [15]. On Pt(110), the reconstruction was very large, probably changing the terrace structures too. On Pt(110)-oriented Pt(431), the change in surface structure was larger than Pt(111)-oriented surfaces, but much smaller than Pt(110), in spite of the largest numbers of steps and kinks, probably because of the less structural irregularity and smaller surface energy compared with Pt(110)–(1 × 1). On Pt(100)-related surfaces, the electro-oxidation of bulk CO proceeded at lower potentials than on other surfaces (Table 1). Especially on Pt(100), the onset potential was as low as 0.29 V. The unstable Pt adatoms or clusters were proposed to exist on the surface.

The potential-step measurements were carried out on Pt(111) in CO-saturated $HClO_4$. At 0.95 V, the Pt atoms with low CNs were preferentially oxidized, which was then reduced to $Pt(CO)_4^{2+}$ or $Pt(CO)_2$ upon the potential step to 0.60 V. $Pt(CO)_4^{2+}$ was immobile at 0.60 V and inactive towards the bulk CO electro-oxidation. At 0.05 V, only $Pt(CO)_2$ existed as a single Pt species on the surface, which were mobile and decreased its CN by the self-deposition at a stable site; the surface reactivity thus decreased. On pure Pt electrodes, unfortunately, it seems improbable to maintain the "low-potential CO oxidation current" after potential cycles in CO-saturated $HClO_4$. The active sites, allowing the adsorption of water molecules through the CO adlayer [15], must be structurally maintained eventually by a surface modification, such as by alloying.

The systematic investigation of the atomically-arranged defects on electrodes has started only recently [15,16]. The combination of defects and adsorbates may create highly-active sites, but are very small in number. As reported in this paper, those created sites could be unstable and changeable too. New analytical technologies and theoretical backbones must be established and applied to this new field.

Supplementary Materials: The following are available online at www.mdpi.com/xxx/s1, Figure S1. Schematic illustration of the adjustment of (111) and (100) facets by a laser beam reflection method. Figure S2. Schematic illustration of a tree-compartment cell. The electrochemical measurements were carried out with the hanging meniscus method.

Author Contributions: Conceptualization, J.I.; methodology, H.U. and J.I.; validation, H.U. and J.I.; investigation, K.A.; resources, H.U. and J.I.; writing—original draft preparation, J.I.; writing—review and editing, H.U. and J.I.; visualization, K.A. and J.I.; supervision, H.U. and J.I.; project administration, J.I.; funding acquisition, J.I.

Funding: This study was supported by Grant-in-Aid for Scientific Research (KAKENHI) and the New Energy and Industrial Technology Development Organization (NEDO), Japan.

Acknowledgments: The authors thank Prof. Nagakazu Furuya of the University of Yamanashi for the stepped-sample preparation

Conflicts of Interest: The authors declare no conflict of interest.

References

1. Markovic, N.M.; Ross, P.N. Surface science studies of model fuel cell electrocatalysts. *Surf. Sci. Rep.* **2002,** *45*, 117–229.
2. Koper, M.T.M.; Lai, S.C.S.; Herrero, E. Mechanisms of the Oxidation of Carbon Monoxide and Small Organic Molecules at Metal Electrodes. In *Fuel Cell Catalysis*; John Wiley & Sons, Inc.: Hoboken, NJ, USA, 2008; pp. 159–207.
3. Korzeniewski, C.; Climent, V.; Feliu, J.M. Electrochemistry at Platinum Single Crystal Electrodes. In *Electrochemistry: A Series of Advances*; Bard, A.J., Zoski, C., Eds.; CRC Press: Boca Raton, FL, USA, 2012; Volume 24; pp. 75–169.
4. Li, Q.-X.; Huo, S.-J.; Ma, M.; Cai, W.-B.; Osawa, M. Ubiquitous Strategy for Probing ATR Surface-Enhanced Infrared Absorption at Platinum Group Metal−Electrolyte Interfaces. *J. Phys. Chem. B* **2005**, *109*, 7900–7906.
5. Atkins, P.W. *Physical Chemistry*, 6th ed.; Oxford University Press: Oxford, UK, 1998.
6. Lopez-Cudero, A.; Cuesta, A.; Gutierrez, C. Potential dependence of the saturation CO coverage of Pt electrodes: The origin of the pre-peak in CO-stripping voltammograms. Part 2: Pt(100). *J. Electroanal. Chem.* **2006**, *586*, 204–216.
7. Lopez-Cudero, A.; Cuesta, A.; Gutierrez, C. Potential dependence of the saturation CO coverage of Pt electrodes: The origin of the pre-peak in CO-stripping voltammograms. Part 1: Pt(111). *J. Electroanal. Chem.* **2005**, *579*, 1–12.
8. Lebedeva, N.P.; Koper, M.T.M.; Herrero, E.; Feliu, J.M.; van Santen, R.A. Cooxidation on stepped Pt[n(111)×(111)] electrodes. *J. Electroanal. Chem.* **2000**, *487*, 37–44.
9. Lebedeva, N.P.; Koper, M.T.M.; Feliu, J.M.; van Santen, R.A. Role of Crystalline Defects in Electrocatalysis: Mechanism and Kinetics of CO Adlayer Oxidation on Stepped Platinum Electrodes. *J. Phys. Chem. B* **2002**, *106*, 12938–12947.
10. Lebedeva, N.P.; Rodes, A.; Feliu, J.M.; Koper, M.T.M.; van Santen, R.A. Role of Crystalline Defects in Electrocatalysis: CO Adsorption and Oxidation on Stepped Platinum Electrodes as Studied by in situ Infrared Spectroscopy. *J. Phys. Chem. B* **2002**, *106*, 9863–9872.
11. Chen, Q.-S.; Berna, A.; Climent, V.; Sun, S.-G.; Feliu, J.M. Specific reactivity of step sites towards CO adsorption and oxidation on platinum single crystals vicinal to Pt(111). *Phys. Chem. Chem. Phys*. **2010**, *12*, 11407.
12. Farias, M.J.S.; Camera, G.A.; Feliu, J.M. Understanding the CO Preoxidation and the Intrinsic Catalytic Activity of Step Sites in Stepped Pt Surfaces in Acidic Medium. *J. Phys. Chem. C* **2015**, *119*, 20272–20282.
13. Mayrhofer, K.J.J.; Blizanac, B.B.; Arenz, M.; Stamenkovic, V.R.; Ross, P.N.; Markovic, N.M. The Impact of Geometric and Surface Electronic Properties of Pt-Catalysts on the Particle Size Effect in Electrocatalysis. *J. Phys. Chem. B* **2005**, *109*, 14433–14440.
14. Marković, N.M.; Grgur, B.N.; Lucas, C.A.; Ross, P.N. Electrooxidation of CO and H_2/CO Mixtures on Pt(111) in Acid Solutions. *J. Phys. Chem*. B **1999**, *103*, 487–495.

15. Inukai, J.; Tryk, D.A.; Abe, T.; Wakisaka, M.; Uchida, H.; Watanabe, M. Direct STM Elucidation of the Effects of Atomic-Level Structure on Pt(111) Electrodes for Dissolved CO Oxidation. *J. Am. Chem. Soc.* **2013**, *135*, 1476–1490.
16. Strmcnik, D.S.; Tripkovic, D.V.; van der Vliet, D.; Chang, K.C.; Komanicky, V.; You, H.; Karapetrov, G.; Greeley, J.; Stamenkovic, V.R.; Markovic, N.M. Unique Activity of Platinum Adislands in the CO Electrooxidation Reaction. *J. Am. Chem. Soc.* **2008**, *130*, 15332–15339.
17. Somorjai, G.; Li, Y. *Introduction to Surface Chemistry and Catalysis*, 2nd ed.; John Wiley & Sons: Hoboken, NJ, USA, 2010.
18. Batista, E.A.; Iwasita, T.; Viestich, W. Mechanism of Stationary Bulk CO Oxidation on Pt(111) Electrodes. *J. Phys. Chem. B* **2004**, *108*, 14216–14222.
19. Rednev, A.V.; Wandlowski, T. An influence of pretreatment conditions on surface structure and reactivity of Pt(100) towards CO oxidation reaction. *Russ. J. Electrochem.* **2012**, *72*, 259–270.
20. Itaya, K. In situ scanning tunneling microscopy in electrolyte solutions. *Prog. Surf. Sci.* **1998**, *58*, 121–247.
21. Wakisaka, M.; Ohkanda, T.; Yoneyama, T.; Uchida, H.; Watanabe, M. Structures of a CO adlayer on a Pt(100) electrode in HClO4 solution studied by in situ STM. *Chem. Commun.* **2005,** 2710–2712, doi:10.1039/b503148f.
22. Wakisaka, M.; Asizawa, S.; Yoneyama, T.; Uchida, H.; Watanabe, M. In Situ STM Observation of the CO Adlayer on a Pt(110) Electrode in 0.1 M HClO4 Solution. *Langmuir* **2010**, *26*, 9191–9194.
23. Furuya, N.; Koide, S. Hydrogen adsorption on platinum single-crystal surfaces. *Surf. Sci.* **1989**, *220*, 18–28.
24. Huerta, F.; Mollaron, E.; Quijada, C.; Vezquez, J.L.; Perez, J.M.; Aldaz, A. The adsorption of methylamine on Pt single crystal surfaces. *J. Electroanal. Chem.* **1999**, *467*, 105–111.
25. Dederichs, F.; Friedrich, K.A.; Daum, W. Sum-Frequency Vibrational Spectroscopy of CO Adsorption on Pt(111) and Pt(110) Electrode Surfaces in Perchloric Acid Solution: Effects of Thin-Layer Electrolytes in Spectroelectrochemistry. *J. Phys. Chem. B* **2000**, *104*, 6626–6632.
26. Wakisaka, M.; Morishima, S.; Hyuga, Y.; Uchida, H.; Watanabe, M. Electrochemical behavior of Pt–Co(111), (100) and (110) alloy single-crystal electrodes in 0.1 M HClO4 and 0.05 M H2SO4 solution as a function of Co content. *Electrochem. Commun*. **2012**, *18*, 55–57.
27. Sashikata, K.; Sugata, T.; Sugimasa, M.; Itaya, K. In Situ Scanning Tunneling Microscopy Observation of a Porphyrin Adlayer on an Iodine-Modified Pt(100) Electrode. *Langmuir* **1998**, *14*, 2896–2902.
28. Kibler, L.A.; Cuesta, A.; Kleinert, M.; Kolb, D.M. In-situ STM characterisation of the surface morphology of platinum single crystal electrodes as a function of their preparation. *J. Electroanal. Chem.* **2000**, *484*, 73–82.
29. Arenz, M.; Mayrhofer, K.J.J.; Stamenkovic, V.; Blizanac, B.B.; Tomoyuki, T.; Ross, P.N.; Markovic, N.M. The Effect of the Particle Size on the Kinetics of CO Electrooxidation on High Surface Area Pt Catalysts. *J. Am. Chem. Soc.* **2005**, *127*, 6819–6829.
30. Giz, M.J.; Batista, E.A.; Vielstich, W.; Iwasita, T. A topographic view of the Pt(111) surface at the electrochemical interface in the presence of carbon monoxide. *Electrochem. Commun.* **2007**, *9*, 1083–1085.

© 2019 by the authors. Licensee MDPI, Basel, Switzerland. This article is an open access article distributed under the terms and conditions of the Creative Commons Attribution (CC BY) license (http://creativecommons.org/licenses/by/4.0/).